

# Unified Unsupervised and Sparsely-Supervised 3D Object Detection by Semantic Pseudo-Labeling and Prototype Learning

Yushen He

Shanghai Jiao Tong University, Shanghai, China

**Abstract.** 3D object detection is essential for autonomous driving and robotic perception, yet its reliance on large-scale manually annotated data limits scalability and adaptability. To reduce annotation dependency, unsupervised and sparsely-supervised paradigms have emerged. However, they face intertwined challenges: low-quality pseudo-labels, unstable feature mining, and a lack of a unified training framework. This paper proposes SPL, a unified training framework for both Unsupervised and Sparsely-Supervised 3D Object Detection via Semantic Pseudo-labeling and prototype Learning. SPL first generates high-quality pseudo-labels by integrating image semantics, point cloud geometry, and temporal cues, producing both 3D bounding boxes for dense objects and 3D point labels for sparse ones. These pseudo-labels are not used directly but as probabilistic priors within a novel, multi-stage prototype learning strategy. This strategy stabilizes feature representation learning through memory-based initialization and momentum-based prototype updating, effectively mining features from both labeled and unlabeled data. Extensive experiments on KITTI and nuScenes datasets demonstrate that SPL significantly outperforms state-of-the-art methods in both settings. Our work provides a robust and generalizable solution for learning 3D object detectors with minimal or no manual annotations.

**Keywords:** 3D Object Detection · Unsupervised Learning · Sparsely-Supervised Learning · Prototype Learning

## 1 Introduction

3D object detection is a critical perception task for applications like autonomous driving and robot navigation, aiming to locate objects within 3D space from sensor inputs such as LiDAR or cameras. While fully-supervised methods [6, 19, 25, 37] have advanced significantly by leveraging large-scale annotated datasets (e.g., KITTI [8], nuScenes [4], Waymo [29]), acquiring accurate 3D bounding box annotations remains costly and labor-intensive. This practical limitation has spurred research into two alternative paradigms: unsupervised and sparsely-supervised 3D object detection.

Unsupervised methods avoid human annotations entirely by generating 3D Bbox pseudo labels from data itself. Some methods [34, 41] exploit geometric

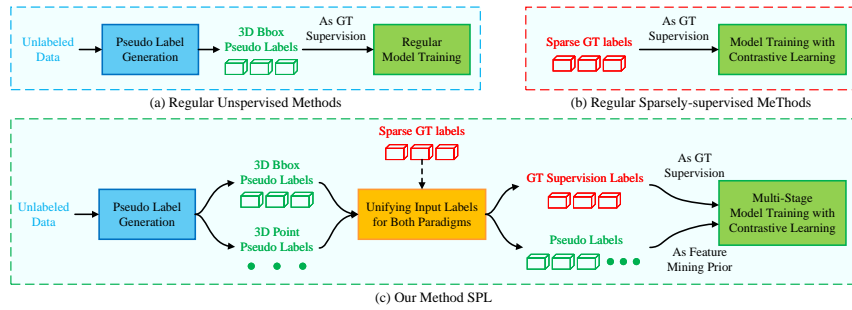


**Fig. 1:** Comparison between existing unsupervised and sparsely-supervised 3D object detection methods and our proposed SPL framework.

features and commonsense priors in point clouds. Other methods utilize either temporal motion cues [3, 33, 40] or projected 2D image semantics [10, 28, 31] to generate pseudo labels. A few methods [13, 42] combine both motion and semantic information. Unsupervised methods primarily focus on improving the quality of generated pseudo labels to enhance detection accuracy.

Sparsely-supervised methods, in contrast, utilize a very limited set of human annotations — only a small subset of training samples are labeled, and each may contain only a single object annotation. These methods typically employ specialized training strategies, such as contrastive learning [35, 48], to enable the model to learn from sparse supervision and generalize to unlabeled objects. An effective training strategy enables sparsely-supervised methods to maintain high performance despite using only sparse annotations.

Despite their promise, both paradigms face fundamental and interrelated challenges:

(1) Low-quality pseudo labels in unsupervised learning. Motion-based methods [3, 33, 40] fail on stationary or slow-moving objects and struggle with class distinction. Methods [10, 28, 31] relying on image semantics suffer from projection errors and background clutter, and generally do not utilize temporal information effectively. Hybrid approaches like LiSe [42] and UNION [13] still inherit the respective limitations of each type of methods. Furthermore, for objects with sparse point clouds, these methods struggle to generate pseudo labels or produce severely mis-sized pseudo labels.

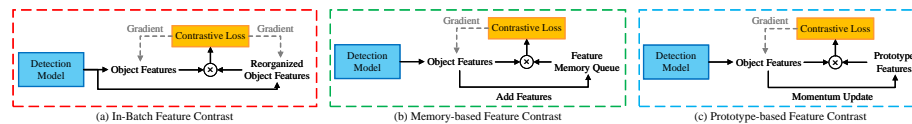


**Fig. 2:** Different contrastive learning strategies in sparsely-supervised 3D object detection.

(2) Unstable feature mining in sparsely-supervised learning. Current strategies based on contrastive learning exhibit significant limitations in sparse settings, as categorized in Fig. 2: (a) In-batch feature contrast (e.g., CoIn [35]) uses only the limited object features available in a batch to construct pairs, leading to unstable training due to inadequate sample diversity. (b) Feature memory queue maintains a fixed-length queue for contrast. While mitigating sample scarcity, it introduces inconsistency as older stored features become outdated relative to the evolving model. (c) Prototype-based contrast (e.g., CPDet3D [48]) employs multiple prototypes each class to represent class features for stable comparison. Contrastive loss is computed between current object features and prototypes, and prototypes are updated via momentum using current features. However, its common random prototype initialization is detrimental to proper prototype learning. These inherent shortcomings in existing contrastive learning strategies result in sub-optimal feature discrimination and representation learning.

(3) Lack of a unified training framework adaptable to both paradigms. Existing approaches are narrowly designed for one setting and fail to leverage the synergy between pseudo label quality and feature mining. In unsupervised training, most methods [3, 13, 31, 34, 40–42] focus mainly on generating high-quality pseudo labels. A few others [28, 33] incorporate auxiliary cues from pseudo labels to optimize loss computation but still do not engage in deep model representation learning. Conversely, in sparsely-supervised training, works like [35, 48] concentrate solely on designing feature mining strategies using the sparse ground truth. However, high-quality pseudo labels and robust feature mining are complementary and crucial for both settings.

To address these challenges, we propose SPL, a unified training framework centered on Semantic Pseudo-Labeling and Prototype Learning, which is simultaneously adaptable to both unsupervised and sparsely-supervised 3D object detection. As shown in Fig. 1, SPL first generates high-quality pseudo labels based on image semantics, then trains the model through a multi-stage strategy centered on prototype learning.

For Challenge 1, we introduce a high-quality pseudo label generation method. It begins with 3D instance segmentation derived from image semantics and point cloud projection. We then employ point cloud geometric features to resolve mis-assigned, missing, and overlapping points. For objects with low point density, we record them as 3D point pseudo labels. For others, we fit 3D Bboxes, refine them using temporal information. Thus it produces both high-quality 3D Bbox pseudo labels and point-level labels for sparse objects.

For Challenge 2, we design a multi-stage prototype learning strategy for stable feature mining. In Stage 1, we use a feature memory queue (Fig. 2(b)) to gather diverse features and initialize prototypes via clustering. Stage 2 adopts a prototype-based strategy (Fig. 2(c)), updating prototypes conservatively using only ground-truth features. Stage 3 further introduces pseudo heatmap priors for comprehensive feature mining, incorporating background contrast to enhance representation learning.

For Challenge 3, we unify the input supervision for both paradigms. We define two label types: “GT Supervision Labels” and “Pseudo Labels”. For sparsely-supervised training, normal inputs are used. For unsupervised training, an evaluation score converts high-quality pseudo labels into “GT Supervision Labels”, with the rest treated as “Pseudo Labels”. Crucially, pseudo labels do not serve as direct supervision. Instead, they act as pseudo heatmap priors, together with prototypes, to guide the feature mining process alongside prototypes. This effectively coupling pseudo label information with representation learning.

Our contributions are summarized as follows:

- We propose SPL, a unified training framework based on Semantic Pseudo-Labeling and Prototype Learning, adaptable to both unsupervised and sparsely-supervised 3D object detection.
- We introduce a high-quality pseudo label generation strategy that combines image semantics, point cloud geometry, and temporal information, producing not only high-quality 3D Bbox pseudo labels for dense objects but also 3D point pseudo labels for sparse objects.
- We design a multi-stage training strategy centered on prototype learning, which unifies unsupervised and sparsely-supervised inputs via an evaluation score, couples pseudo labels with feature mining through pseudo heatmap priors, and stabilizes prototype initialization and updating while promoting deep representation learning.
- Extensive experiments on KITTI and nuScenes datasets demonstrate that our method outperforms existing approaches in both unsupervised and sparsely-supervised 3D object detection tasks.

## 2 Related Work

### 2.1 Fully-Supervised 3D Object Detection

3D object detection primarily takes LiDAR point clouds as input. VoxelNet [47] first uses neural network for this task by voxelizing point clouds, with subsequent works like SECOND [38] and CenterPoint [39] improving the model. Then some methods [11] focus on achieving faster inference speeds, while others [6, 25] enhance accuracy through two-stage frameworks. Additionally, some works [17, 18, 24] explore camera-only detection to reduce sensor costs, while multi-modal methods [19, 26, 37] fuse LiDAR and camera data for higher performance. Despite their strong performance, these approaches rely heavily on large-scale, accurately annotated 3D datasets, which limits their scalability and adaptability across different environments, sensor setups, and platforms.

### 2.2 Unsupervised 3D Object Detection

Early unsupervised methods [2, 23, 27] produce detection results via non-learning strategies. More recent methods generally follow a two-stage pipeline: first generating pseudo 3D Bbox labels from unlabeled data, and then training a detector with these pseudo labels. Existing methods can be categorized based on

their pseudo label generation mechanisms: (1) Geometry-based methods [34, 41] exploit geometric cues and common-sense priors from point clouds. (2) Motion-based methods [3, 33, 40] leverage motion cues across consecutive frames to identify moving objects. (3) Image-semantic-based methods [10, 28, 31] project 3D point cloud to 2D image to obtain semantic segmentation. (4) Hybrid methods [13, 42] combine both motion and semantic information. However, the quality of generated pseudo labels remains a bottleneck. Moreover, these methods lack training strategy that encourage the learning of discriminative representations.

### 2.3 Sparsely-Supervised 3D Object Detection

SS3D [16] pioneers sparsely-supervised 3D detection by employing GT Sampling and self-training. CoIn [35] introduces contrastive learning using object features within mini-batches to mine features for unlabeled objects. HINTED [36] extends CoIn with a mixed-feature augmentation strategy. CPDet3D [48] adopts a prototype-based contrastive learning for efficient feature representation. SP3D [45] attempts to enrich the sparse ground truth by generating additional pseudo labels. However, their feature mining strategies — often based on contrastive learning — still face issues of training instability. Furthermore, they do not integrate pseudo labels into the feature mining process.

### 2.4 Prototype-based Methods

Prototype-based methods [14, 20, 32, 44] have been widely explored in 2D object detection and representation learning. In 3D detection, Some works [15, 21, 46] utilize geometric prototypes for tasks such as unsupervised and domain-adaptive detection. MoCo [9] introduces a momentum update mechanism for maintaining consistent feature queues in contrastive learning. CPDet3D [48] adapts ideas from MoCo and uses for feature-level prototype learning in sparsely-supervised 3D detection. Our method draws inspiration from MoCo and CPDet3D.

## 3 Method

We propose SPL, a unified training framework that is simultaneously adaptable to both unsupervised and sparsely-supervised 3D object detection. SPL first generates high-quality 3D Bbox pseudo labels by integrating image semantics, point cloud geometry, and temporal cues, and additionally produces 3D point pseudo labels for objects with sparse point clouds. It then unifies the input supervision for both paradigms into two types: “GT supervision labels” and “pseudo labels”. The training framework employs a prototype-based training strategy to train the 3D object detector, and adopts a multi-stage training scheme to achieve stable and effective representation learning.

We now present the details of our approach. In Sec. 3.1, we describe our 3D pseudo label generation strategy. Sec. 3.2 introduces the prototype-based training strategy at the core of our framework. Finally, Sec. 3.3 elaborates on the multi-stage training pipeline implemented in SPL.

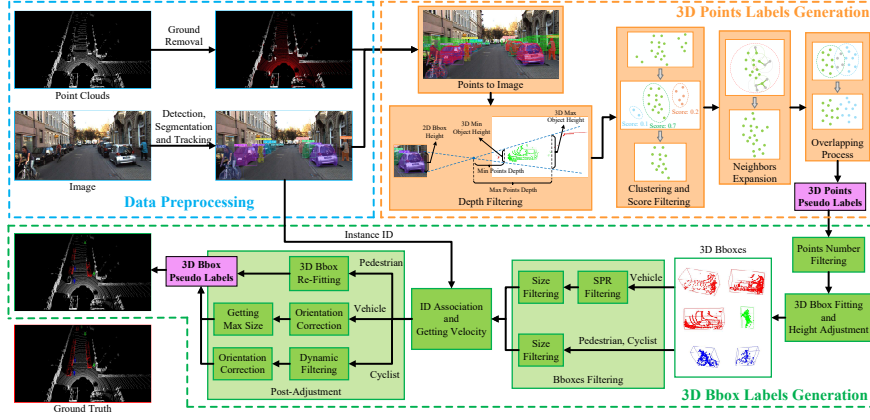


Fig. 3: Overview of the 3D pseudo label generation process.

### 3.1 3D Pseudo Label Generation

This section presents our method for generating high-quality 3D pseudo labels. As illustrated in Fig. 3, the process takes point clouds and images of a continuous scene as input, and proceeds through three sequential stages: Data Preprocessing, 3D Point Labels Generation, and 3D Bbox Labels Generation, yielding 3D pseudo labels for each frame.

**Data Preprocessing:** We begin by preprocessing raw point clouds and images. For LiDAR point clouds, we aggregate multi-frame data using ego-vehicle poses and remove ground points via the Patchwork++ algorithm [12]. For RGB images, to ensure efficiency, we employ the detector YOLOv12 [30] coupled with the tracker BoT-SORT [1] to obtain per-frame object class labels  $C^t = [c_1^t, c_2^t, \dots]$ , 2D Bboxes  $B^t = [b_1^t, b_2^t, \dots]$ , instance segmentation masks  $M^t = [m_1^t, m_2^t, \dots]$ , and consistent cross-frame object IDs. This process is shown in Eq. (1), where  $I^t$  denotes the image at frame  $t$ . The object classes (Vehicle, Pedestrian, Cyclist) align with common autonomous driving benchmarks.

$$[C^t, B^t, M^t, ID^t] = f_{det+track}(I^t) \quad (1)$$

**3D Points Labels Generation:** This stage aims to generate reliable 3D point pseudo labels by fusing 2D image semantics with 3D point cloud geometry.

First, we project the ground-removed point cloud  $Pc^t$  onto the image plane to obtain  $Pc_{im}^t$ . For each 2D object  $i$  with associated  $[c_i^t, b_i^t, m_i^t]$ , we extract points in  $Pc_{im}^t$  falling within its mask  $m_i^t$  as the corresponding point cloud  $pc_i^t$ . The mask  $m_i^t$  is dilated to include more points.

For each object category  $c$ , we define a real-world height range  $[h_{c,\min}, h_{c,\max}]$ . Given the pixel height  $h_i^t$  of object  $i$  in the image, the depth range  $[d_{i,\min}^t, d_{i,\max}^t]$

of its point cloud is computed by Eq. (2), where  $f_y$  is the camera’s vertical focal length. We filter out points in  $pc_i^t$  that fall outside this depth range.

$$d_{i,min}^t = \frac{f_y \cdot h_{c,min}}{h_i^t}, \quad d_{i,max}^t = \frac{f_y \cdot h_{c,max}}{h_i^t} \quad (2)$$

We then address misassigned, missing, and overlapping points in  $pc_i^t$  through the following steps:

1. Removing misassigned points: We cluster  $pc_i^t$  using DBSCAN [7] into sub-clusters  $[pc_{i,1}^t, pc_{i,2}^t, \dots]$ . A fitting score for each subcluster is computed by Eq. (3), considering both the proportion of points within the image mask and the cluster size. The subcluster with the highest score is retained as the updated  $pc_i^t$ .

$$score(k) = \frac{|\{p \in pc_{i,k}^t | p \in m_i^t\}|}{|pc_{i,k}^t|} + \frac{|pc_{i,k}^t|}{\max_j |pc_{i,j}^t|} \quad (3)$$

2. Recovering missing points: Given a search radius  $r_1$  and a maximum radius  $r_2$ , we iteratively add points within  $r_1$  of the current  $pc_i^t$  and within  $r_2$  of  $pc_i^t$ ’s initial centroid until no further points can be added.
3. Resolving point ownership conflicts: For points claimed by multiple objects, a K-nearest neighbor majority voting algorithm [22] determines the final ownership based on the predominant object label in their neighborhood.

After these steps, each object  $i$  is associated with a refined point cloud  $pc_i^t$ . Its centroid  $p_i^t$  is then recorded as the 3D point pseudo label.

**3D Bbox Labels Generation:** Based on the 3D point pseudo labels, we generate 3D Bbox pseudo labels and refine them using temporal consistency.

First, for each object  $i$ , if the number of its corresponding points  $|pc_i^t|$  exceeding a threshold, a 3D Bbox  $b_{3d,i}^t = [x, y, z, l, w, h, \theta]$  is estimated via the L-shape fitting algorithm [43], with its height adjusted to ground contact. 3D Bboxes with unreasonable length, width, or height are filtered out. For Vehicle objects, we further compute the Surface Proximity Ratio (SPR)—the proportion of points lying close to the box surface, and discard Bboxes with low SPR.

Next, we use the object IDs obtained during image preprocessing for cross-frame association. For object  $i$  present in consecutive frames, its velocity  $v_i^t$  is computed using the centroid displacement via Eq. (4), where  $\Delta p_i^{t-1} = p_i^t - p_i^{t-1}$ ,  $\Delta p_i^t = p_i^{t+1} - p_i^t$ , and  $\Delta t_{t-1}$ ,  $\Delta t_t$  are inter-frame time intervals.

$$v_i^t = \frac{\Delta p_i^{t-1} \cdot \Delta t_t + \Delta p_i^t \cdot \Delta t_{t-1}}{\Delta t_{t-1} + \Delta t_t} \quad (4)$$

Finally, we integrate motion cues to refine the 3D Bboxes: (1) For Pedestrian objects, the 3D Bbox orientation is aligned with the velocity direction, and the Bbox is refitted accordingly. (2) For Vehicle and Cyclist objects, 3D Bboxes with an orientation deviating more than 90 degrees from the velocity direction

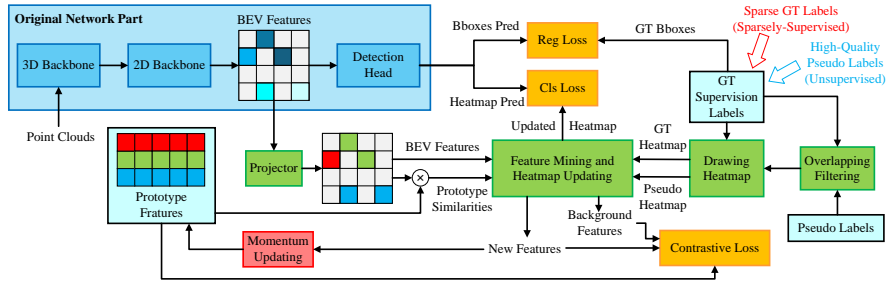


Fig. 4: Overview of the prototype-based training strategy.

are reversed. (3) To counteract undersized Bboxes due to partial scanning, vehicle dimensions are set to the maximum observed over consecutive frames. (4) Stationary Cyclist Bboxes are removed to avoid taking the parking ridings as valid detections.

In summary, high-quality 3D Bbox pseudo labels are produced for well-scanned objects, while 3D point pseudo labels are retained for sparse objects, ensuring their participation in subsequent training.

### 3.2 Prototype-Based Training Strategy

We build our prototype-based training strategy upon a conventional 3D detection architecture. We adopt CenterPoint [39] as the baseline detector, modifying only its loss computation while leaving the inference network unchanged. Our strategy is also applicable to other detectors, such as the two-stage detector Voxel-RCNN [6] and the multimodal detectors BEVFusion [19], provided they using heatmap for classification loss calculation like CenterPoint.

As illustrated in Fig. 4, the core of our approach lies in maintaining and updating a set of prototypes  $P \in \mathbb{R}^{C \times K \times D}$ , where  $C$ ,  $K$ , and  $D$  denote the number of object classes, prototypes per class, and feature dimension respectively. During training, we encourage intermediate BEV features to align with corresponding prototypes while leveraging pseudo labels as additional guidance for feature mining. In the following, we detail our training strategy, covering Labels Processing, Feature Mining, Loss Function, and Prototype Update.

**Labels Processing:** We define two label types for both training paradigms: “GT Supervision Labels” and “Pseudo Labels”. For sparsely-supervised training, sparse human annotations serve as “GT Supervision Labels”. For unsupervised training, we convert high-quality 3D Bbox pseudo labels into “GT Supervision Labels”. Quality is measured by high 2D-3D alignment (IoU between projected 3D Bbox and 2D mask) and evidence of dynamic motion. Both 3D Bbox and 3D point pseudo labels (after removing overlaps with GT Supervision Labels) are collected as “Pseudo Labels”.

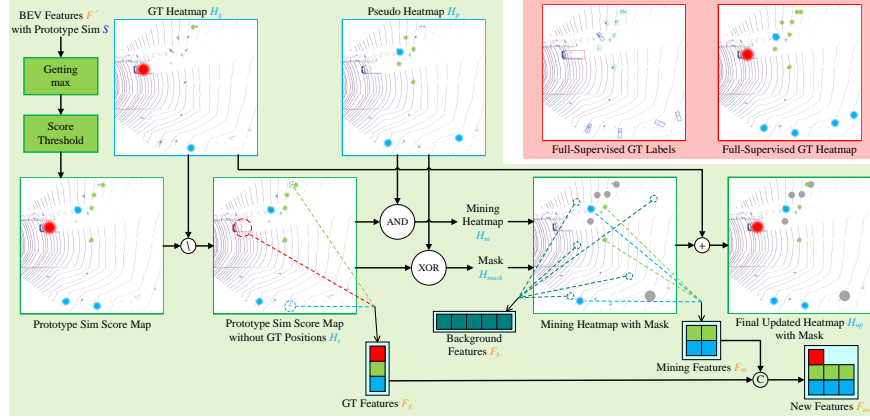


**Fig. 5:** Feature mining process combining prototype similarity and pseudo heatmap.

We generate a GT heatmap  $H_g$  from GT Supervision Labels and a pseudo heatmap  $H_p$  from Pseudo Labels using the standard heatmap generation procedure of CenterPoint. Since 3D point pseudo labels lack size, we assign them the minimum size of their respective class.

**Feature Mining:** The Feature Mining step identifies potential unlabeled objects by combining prototype similarity and pseudo heatmap priors. Given intermediate BEV features  $F$ , we project them through a small network  $\text{Proj}(\cdot)$  consisting of a 2D convolution followed by L2 normalization, yielding  $F' = \text{Proj}(F) \in \mathbb{R}^{H \times W \times D}$ , where  $H$  and  $W$  are the spatial dimensions of the feature map. Because both  $F'$  and the prototypes  $P$  are normalized, we compute their cosine similarity  $S \in \mathbb{R}^{H \times W \times C \times K}$  via dot product:

$$S(h, w, c, k) = F'(h, w) \cdot P(c, k), \quad h \in [1, H], w \in [1, W], c \in [1, C], k \in [1, K] \quad (5)$$

The following processing is shown in Fig. 5. We reduce  $S$  by taking the maximum similarity at each spatial location, producing  $S' \in \mathbb{R}^{H \times W}$  along with corresponding classes  $C_{id}^s \in \mathbb{R}^{H \times W}$  and prototype indices  $K_{id}^s \in \mathbb{R}^{H \times W}$ :

$$S'(h, w) = \max_{c, k} S(h, w, c, k), \quad C_{id}^s(h, w), K_{id}^s(h, w) = \arg \max_{c, k} S(h, w, c, k) \quad (6)$$

We filter low-confidence locations by a fixed threshold  $\tau_s$ , and exclude areas already occupied by GT objects, yielding a similarity score map  $H_s$ :

$$H_s(h, w) = \begin{cases} S'(h, w), & \text{if } S'(h, w) > \tau_s \text{ and } H_g(h, w) = 0 \\ 0, & \text{otherwise} \end{cases} \quad (7)$$

Then we fuse  $H_s$  with the pseudo heatmap  $H_p$  using two rules: (1) positions where both  $H_p$  and  $H_s$  are positive and class predictions agree receive positive supervision; (2) positions where either  $H_p$  or  $H_s$  is positive (but not both)

are masked out from negative supervision to avoid suppressing potentially correct predictions. Formally, the mining heatmap  $H_m$  (positive signals) and the mask  $H_{mask}$  (ambiguous regions) are obtained by Eq. (8) and Eq. (9). The final heatmap used for classification supervision is then  $H_{up} = H_g + H_m$ .

$$H_m(h, w) = \begin{cases} H_s(h, w), & \text{if } H_p(h, w) > 0 \text{ and } H_s(h, w) > 0 \text{ and } C_{id}^s(h, w) = C_{id}^p(h, w) \\ 0, & \text{otherwise} \end{cases} \quad (8)$$

$$H_{mask}(h, w) = \begin{cases} 0, & \text{if } (H_p(h, w) > 0 \text{ or } H_s(h, w) > 0) \text{ and } H_m(h, w) = 0 \\ 1, & \text{otherwise} \end{cases} \quad (9)$$

Furthermore, we extract feature vectors at the locations marked by  $H_g$  and  $H_m$  to form the set of foreground features  $F_{new} = [F_g; F_m]$ , where

$$F_g = \{F'(h, w) | H_g(h, w) > 0\}, \quad F_m = \{F'(h, w) | H_m(h, w) > 0\} \quad (10)$$

We also collect the class indices  $C_{id}^{new}$  and prototype indices  $K_{id}^{new}$  of  $F_{new}$ . For  $F_g$  part, the class indices are derived from the GT labels, and the prototype indices are the ones with the highest similarity. For  $F_m$  part, both indices are obtained from Eq. (6).

To strengthen the contrastive learning, we randomly sample a set of background features  $F_{bg}$  by Eq. (11), where  $|F_{bg}| = C \times K$ .

$$F_{bg} = \text{Sample}(\{F'(h, w) | H_g(h, w) = 0 \text{ and } H_p(h, w) = 0 \text{ and } H_s(h, w) = 0\}) \quad (11)$$

**Loss Function:** The overall training loss comprises four components:

$$L = L_{reg} + L_{cls} + \lambda_1 L_{con,intra} + \lambda_2 L_{con,inter} \quad (12)$$

The regression loss  $L_{reg}$  follows CenterPoint’s original formulation, using only the sparse “GT Supervision Labels”. We find that even with few GT Bboxes, the model learns to predict reasonable 3D Bboxes.

The classification loss  $L_{cls}$  is adapted from CenterPoint: the target heatmap is replaced by  $H_{up}$ , and the loss is computed only where  $H_{mask} = 1$  (ambiguous regions excluded).

The intra-class contrastive loss  $L_{con,intra}$  is defined in Eq. (13), where  $\tau_t$  is the temperature parameter, which pulls each foreground feature toward its assigned prototype while pushing it away from other prototypes of the same class.

$$L_{con,intra} = -\frac{1}{|F_{new}|} \sum_{i=1}^{|F_{new}|} \log \frac{\exp(F_{new,i} \cdot P(C_{id,i}^{new}, K_{id,i}^{new})/\tau_t)}{\sum_{k=1}^K \exp(F_{new,i} \cdot P(C_{id,i}^{new}, k)/\tau_t)} \quad (13)$$

The inter-class contrastive loss  $L_{con,inter}$  is given by Eq. (14), which enhances discrimination across different categories and between foreground and background.

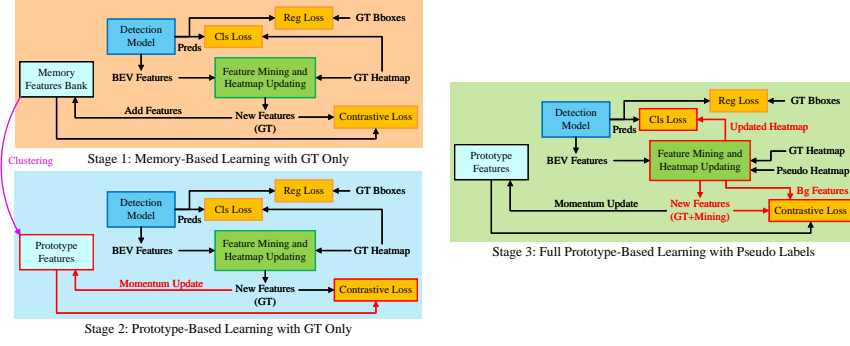


Fig. 6: Overview of the multi-stage training pipeline.

$$L_{con,inter} = -\frac{1}{|F_{new}|} \sum_{i=1}^{|F_{new}|} \log \frac{S_{self}}{S_{proto} + S_{bg}}, \quad S_{self} = \exp(F_{new,i} \cdot P(C_{id,i}^{new}, K_{id,i}^{new})/\tau_t),$$

$$S_{proto} = S_{self} + \sum_{c \neq C_{id,i}^{new}} \sum_{k=1}^K \exp(F_{new,i} \cdot P(c, k)/\tau_t), \quad S_{bg} = \sum_{j=1}^{|F_{bg}|} \exp(F_{new,i} \cdot F_{bg,j}/\tau_t)$$
(14)

**Prototype Updating:** We update the prototypes using a momentum-based approach inspired by MoCo [9]. For each prototype  $P(c, k)$ , we collect all features in  $F_{new}$  assigned to it, denoted as  $F_{c,k} = \{F_{new,i} | C_{id,i}^{new} = c, K_{id,i}^{new} = k\}$ . If  $F_{c,k}$  is non-empty, we compute its mean feature vector  $\bar{F}_{c,k}$  and update the prototype via Eq. (15), where  $\alpha$  is the momentum coefficient.

$$P(c, k) \leftarrow Norm_{L2}(\alpha P(c, k) + (1 - \alpha)\bar{F}_{c,k}), \quad \bar{F}_{c,k} = \frac{1}{|F_{c,k}|} \sum_{f \in F_{c,k}} f \quad (15)$$

In summary, our prototype-based training strategy effectively integrates both GT supervision and pseudo labels to guide feature mining and representation learning. The loss functions encourage discriminative feature learning, while the momentum-based prototype updating ensures stable and consistent prototype representations throughout training.

### 3.3 Multi-Stage Training Pipeline

Direct application of the prototype-based training strategy often leads to unstable prototype learning due to poor initialization and the noisy nature of pseudo labels. To address this, we adopt a three-stage training pipeline that progressively transitions from memory-based feature collection to full prototype-based learning. As shown in Fig. 6, each stage introduces increasingly complex components while maintaining training stability.

**Stage 1: Memory-Based Learning with GT Only.** This stage uses only “GT Supervision Labels”. We adopt a memory-based contrastive learning strategy, maintaining a memory feature bank  $M_c$  for each class  $c$ . During training, we extract features  $F_g$  from GT-labeled objects and compute contrastive loss against stored features in  $M_c$ . For each class  $c$ , the memory bank is updated by enqueueing new features and dequeuing the oldest ones. The contrastive loss in this stage is computed as shown in Eq. (16), where for each feature  $F_{g,i}$ ,  $m_i^+$  is the most similar positive feature from the same class in the memory bank, and  $M_i^-$  contains negative features from other classes. This pulls features of the same class closer while pushing apart features from different classes.

$$L_{con} = -\frac{1}{|F_g|} \sum_{i=1}^{|F_g|} \log \frac{\exp(F_{g,i} \cdot m_i^+ / \tau_t)}{\exp(F_{g,i} \cdot m_i^+ / \tau_t) + \sum_{m_i^- \in M_i^-} \exp(F_{g,i} \cdot m_i^- / \tau_t)} \quad (16)$$

At the end of Stage 1, we perform K-means clustering on the accumulated memory features of each class to initialize the prototypes, providing a robust starting point for subsequent stages.

**Stage 2: Prototype-Based Learning with GT Only.** With prototypes initialized, we now switch to the prototype-based learning strategy while still using only “GT Supervision Labels”. The training process in this stage differs from the full strategy described in Sec. 3.2 in several aspects: (1) The classification loss  $L_{cls}$  is computed in the conventional manner, using only the GT heatmap  $H_g$  as the target. (2) For contrastive learning, only foreground features from GT objects  $F_{new} = F_g$  are used. Neither mined features  $F_m$  nor background features  $F_{bg}$  participate in the contrastive loss computation. (3) Prototype updating uses only the GT foreground features  $F_g$ , without influence from pseudo-labeled or mined regions. This stage focuses on stabilizing the initialized prototypes and learning robust feature representations before introducing pseudo labels in the next stage.

**Stage 3: Full Prototype-Based Learning with Pseudo Labels.** In this final stage, we activate the complete prototype-based training strategy from Sec. 3.2, incorporating both “GT Supervision Labels” and “Pseudo Labels” for comprehensive feature mining and prototype learning.

## 4 Experiments

We evaluate the effectiveness of our SPL framework on KITTI [8] and nuScenes [4] datasets under both unsupervised and sparsely-supervised 3D object detection settings. We compare SPL with recent state-of-the-art methods and conduct ablation studies to validate each component.

#### 4.1 Datasets and Evaluation Metrics

**KITTI Dataset:** The KITTI 3D object detection dataset [8] contains 7,481 training samples. Following common practice, we split them into 3,712 for training and 3,769 for validation. For sparsely-supervised experiments, we adopt the same setting as CoIn [35]: only one object is annotated in 10% of the scene, resulting in approximately 2% of the total annotations. For unsupervised experiments, we use all training samples without any 3D Bbox annotations. Evaluation uses the official Average Precision (AP) at 40 recall positions (R40) for the Car, Pedestrian, and Cyclist classes.

**nuScenes Dataset:** The nuScenes dataset [4] is a large-scale multimodal dataset containing 1000 driving scenes, split into 700 for training, 150 for validation, and 150 for testing. We use the training set (about 28,000 annotated keyframes) for training and the validation set (about 6,000 keyframes) for evaluation. For sparsely-supervised experiments, we follow CoIn [35] and annotate one object per keyframe, resulting in approximately 10% of total annotations. For unsupervised experiments, we consider three major object classes: Vehicle (car, truck, bus, trailer, construction vehicle), Pedestrian, and Cyclist (motorcycle, bicycle). Evaluation uses the official mean Average Precision (mAP) and nuScenes Detection Score (NDS).

#### 4.2 Implementation Details

**Pseudo-Label Generation:** We use YOLOv12 [30] and BoT-SORT [1] for 2D detection and tracking. For DBSCAN [7], the parameter min-samples is 4, and the  $\epsilon$  is set to 0.5m, 0.3m, and 0.3m for Vehicle, Pedestrian, and Cyclist. The search radius  $r_1$  is set to 0.25m, 0.15m, and 0.15m for Vehicle, Pedestrian, and Cyclist, while the maximum radius  $r_2 = 4r_1$ . For Surface Proximity Ratio (SPR), the minimum distance to the box surface is 0.2m, and the SPR threshold is set to 0.8. When converting 3D Bbox pseudo labels to “GT Supervision Labels” for unsupervised training, the IoU threshold for 2D-3D alignment is 0.4.

**Network and Training:** We implement our framework on two base detectors: CenterPoint [39] and Voxel-RCNN [6]. The Voxel-RCNN uses the same one-stage detection head as CenterPoint to apply our prototype-based training strategy, while retaining its original two-stage refinement module and loss functions unchanged. For KITTI experiments, we use Voxel-RCNN as the detector; for nuScenes, we use CenterPoint.

We set the number of prototypes per class  $K = 5$ , feature dimension  $D = 64$ , similarity threshold  $\tau_s = 0.9$ , temperature  $\tau_t = 1.0$ , and momentum coefficient  $\alpha = 0.9$ . The memory bank size in Stage 1 is set to 1000. The loss weights  $\lambda_1$  and  $\lambda_2$  for the intra-class and inter-class contrastive losses are set to 0.5 and 1.0. The model is trained on 4 NVIDIA RTX 3090 GPUs. We use the Adam optimizer and the cosine annealing schedule with an initial learning rate of  $3 \times 10^{-3}$  for

**Table 1:** Comparison on Sparsely-Supervised 3D Object Detection on KITTI val set.

Annotation Rate	Method	Car			Pedestrian			Cyclist		
		AP @ 3D-IoU 0.7			AP @ 3D-IoU 0.5			AP @ 3D-IoU 0.5		
		Easy	Mod.	Hard	Easy	Mod.	Hard	Easy	Mod.	Hard
100%	Voxel-RCNN	92.3	84.9	82.6	69.6	63.0	58.6	88.7	72.5	68.2
	Voxel-RCNN	70.5	54.9	44.8	42.6	38.5	32.1	73.3	47.8	43.2
2%	CoIn	89.1	70.2	55.6	50.8	45.2	39.6	80.2	52.3	48.6
	CoIn++	<b>92.0</b>	79.5	71.5	46.7	36.1	31.2	82.0	58.4	54.6
	SP3D	91.3	80.5	74.0	67.4	58.7	50.9	<b>92.5</b>	<b>73.1</b>	68.3
	SPL (Ours)	91.8	<b>82.2</b>	<b>79.4</b>	<b>69.5</b>	<b>63.2</b>	<b>56.7</b>	91.8	73.0	<b>68.5</b>

**Table 2:** Comparison on Sparsely-Supervised 3D Object Detection on nuScenes val set.

Annotation Rate	Method	mAP	NDS	Car	Truck	C.V.	Bus	Trailer	Barrier	Motor.	Bike	Ped.	T.C.
100%	CenterPoint	56.11	64.61	84.63	52.87	16.40	66.85	36.85	65.79	53.97	35.39	83.46	64.91
10%	CenterPoint	8.09	25.77	24.62	2.84	0.00	15.66	0.00	4.07	3.33	0.29	25.11	4.96
	CoIn	12.47	33.79	38.70	6.85	0.00	20.67	7.81	11.51	2.85	<b>3.36</b>	34.85	8.50
	SPL (Ours)	<b>38.70</b>	<b>48.96</b>	<b>72.41</b>	<b>42.03</b>	<b>21.02</b>	<b>59.11</b>	<b>23.29</b>	<b>47.45</b>	<b>3.94</b>	0.00	<b>70.51</b>	<b>47.22</b>

CenterPoint and  $1 \times 10^{-2}$  for Voxel-RCNN. We apply GT Sampling augmentation during training. For KITTI, the total training epochs are 80 (Stage 1: 10, Stage 2: 10, Stage 3: 60). For nuScenes, the total training epochs are 30 (Stage 1: 5, Stage 2: 5, Stage 3: 20). To further boost performance, we employ a self-training strategy: after training the model with the above pipeline, we use it to generate pseudo labels on the entire training set, and then retrain the detector using these pseudo labels as additional supervision.

For more implementation details for pseudo-label generation and training, please refer to the supplementary material.

### 4.3 Comparison with State-of-the-Art Methods

**Comparison on Sparsely-Supervised 3D Object Detection:** On KITTI (Tab. 1), we compare SPL with CoIn [35] and SP3D [45] under the same 2% annotation setting. All methods use Voxel-RCNN as the base detector. SPL achieves the best performance on most metrics, surpassing SP3D by 2.1% on mean AP across all classes and difficulty levels. On nuScenes (Tab. 2), we compare SPL with CoIn [35] under the same 10% annotation setting, using CenterPoint as the base detector. SPL significantly outperforms CoIn by 26.23% in mAP and 15.17% in NDS. These results validate the superiority of our SPL framework in sparsely-supervised 3D object detection across different datasets and detectors.

**Comparison on Unsupervised 3D Object Detection:** On KITTI (Tab. 3), we compare SPL with several recent unsupervised 3D detection methods, including MODEST [40], OYSTER [41], CPD [34], Motal [33], and LISO [3]. All meth-

**Table 3:** Comparison on Unsupervised 3D Object Detection on KITTI val set.

Train Set	Method	Car			Pedestrian			Cyclist		
		AP @ 3D-IoU 0.5			AP @ 3D-IoU 0.5			AP @ 3D-IoU 0.5		
		Easy	Mod.	Hard	Easy	Mod.	Hard	Easy	Mod.	Hard
Waymo	MODEST	47.6	33.4	30.6	1.3	2.2	2.3	0.1	0.0	0.0
	OYSTER	65.3	54.8	43.6	3.0	3.0	3.0	1.7	1.8	1.9
	CPD	90.9	81.0	79.8	17.1	15.2	14.2	11.1	7.3	6.5
	Motal	<b>96.2</b>	<b>87.6</b>	<b>85.8</b>	37.9	33.4	31.1	56.3	37.8	35.5
KITTI	OYSTER	43.7	34.5	31.2	0.0	0.0	0.0	0.0	0.0	0.0
	LISO	62.4	53.7	45.6	13.4	10.8	8.2	20.4	13.7	10.3
	SPL (Ours)	93.3	83.1	75.9	<b>46.1</b>	<b>40.5</b>	<b>34.0</b>	<b>67.1</b>	<b>41.9</b>	<b>36.7</b>

**Table 4:** Comparison on Unsupervised 3D Object Detection on nuScenes val set.

Method	Detector	mAP	NDS	Vehicle	Pedestrian	Cyclist
UNION	CenterPoint	25.1	24.4	31.0	44.2	0.0
AnnofreeOD	Voxel-NeXt	34.4	36.6	44.1	51.1	<b>7.9</b>
SPL (Ours)	CenterPoint	<b>38.3</b>	<b>40.6</b>	<b>48.1</b>	<b>59.3</b>	7.2

ods use Voxel-RCNN as the base detector. Since KITTI has limited data, many prior works train their models on the larger Waymo dataset [29] and evaluate on KITTI. In contrast, we train SPL directly on the KITTI training set without external data. Despite this, SPL outperforms all compared methods on most metrics, achieving significant improvements in AP for Pedestrian and Cyclist classes. On nuScenes (Tab. 4), we compare SPL with UNION [13] and AnnofreeOD [28], using CenterPoint and Voxel-NeXt [5] as base detectors respectively. Due to the limitations of semantic-based pseudo-label generation, which cannot cover classes like Barrier and Traffic Cone, we only evaluate Vehicle, Pedestrian, and Cyclist classes. SPL achieves the best performance in both mAP and NDS. These results demonstrate the effectiveness of our SPL framework in unsupervised 3D object detection across different datasets and detectors.

For visualizations of detection results and the pseudo labels generated by our method, please refer to the supplementary material.

#### 4.4 Ablation Studies

**Ablation on Pseudo Labels Generation Strategy:** We first conduct ablation studies on the pseudo labels generation strategy using the KITTI dataset. Since pseudo labels are not directly used for supervision in our SPL framework, we evaluate their quality using precision and recall metrics instead of detection performance. As shown in Tab. 5, we compare our full pseudo label generation method with LISO [3] and UNION [13]. Our method achieves significantly higher recall while maintaining competitive precision. We further ablate key components of our strategy: (a) using only 3D Bbox pseudo labels without 3D point pseudo labels results in high precision but low recall; (b) incorporating 3D

**Table 5:** Ablation studies on Pseudo Labels Generation Strategy on KITTI.

Pseudo Labels Generation Method		Precision			Recall		
		Car	Pedestrian	Cyclist	Car	Pedestrian	Cyclist
LISO		61.4	40.3	54.7	24.7	8.1	17.4
UNION		84.5	67.1	64.5	54.1	43.7	41.8
SPL	(a) without 3D point pseudo labels	<b>93.4</b>	<b>84.5</b>	<b>90.7</b>	34.7	21.5	28.6
	(b) with 3D point pseudo labels	82.6	64.3	76.1	<b>67.4</b>	<b>54.9</b>	<b>61.7</b>
	(c) without object points refinement	70.6	57.6	67.8	59.3	47.1	53.7
	(d) without 3D Bboxes refinement	73.4	59.0	70.9	62.4	51.7	57.4

**Table 6:** Ablation studies on Prototype-Based Training Strategy on KITTI val set.

Pseudo heatmap	Prototype sim score map	Contrastive loss	Car	Pedestrian	Cyclist
			(AP @ 3D-IoU 0.7)	(AP @ 3D-IoU 0.5)	(AP @ 3D-IoU 0.5)
			60.2	38.4	52.1
✓			74.1	47.6	61.3
	✓		71.7	45.7	57.0
	✓	✓	77.9	52.7	69.2
✓	✓	✓	<b>85.6</b>	<b>64.1</b>	<b>81.2</b>

point pseudo labels (set to the average size of the respective class) greatly improves recall at the cost of some precision; (c) removing the refinement of object points (addressing misassigned, missing, and overlapping points) degrades both precision and recall; (d) removing the refinement of 3D Bboxes with temporal information also leads to performance drops. These results validate the effectiveness of each component in our pseudo label generation strategy. The 3D Bbox pseudo labels can provide accurate supervision, while the 3D point pseudo labels enhance coverage and diversity for feature learning.

**Ablation on Training Strategy:** We then perform ablation studies on the training strategy. The experiments are conducted on sparsely-supervised setting of KITTI dataset using Voxel-RCNN as the base detector. As shown in Tab. 6, we evaluate the contributions of three key components: (1) the pseudo heatmap  $H_p$  guides the model to focus on reliable pseudo-labeled regions, significantly improving performance over using only GT supervision; (2) the prototype similarity score map  $H_s$  helps mine additional informative features, further boosting detection accuracy; (3) the contrastive loss encourages discriminative feature learning, leading to substantial gains when combined with  $H_s$ . The full combination of all three components yields the best results across all classes.

We also ablate the multi-stage training pipeline in Tab. 7. Training with only Stage 3 (full prototype-based learning) results in suboptimal performance due to unstable prototype learning. Adding Stage 2 (prototype-based learning with GT only) improves stability and performance. Including Stage 1 (memory-based learning with GT only) further enhances prototype initialization and feature representation, leading to the best overall results. These findings validate the

**Table 7:** Ablation studies on Multi-Stage Training Pipeline on KITTI val set.

Stage 1	Stage 2	Stage 3	Car (AP @ 3D-IoU 0.7)	Pedestrian (AP @ 3D-IoU 0.5)	Cyclist (AP @ 3D-IoU 0.5)
		✓	81.3	60.4	77.9
	✓	✓	82.9	61.7	79.1
✓		✓	83.5	62.8	80.7
✓	✓	✓	<b>85.6</b>	<b>64.1</b>	<b>81.2</b>

effectiveness of our multi-stage training approach in stabilizing and enhancing prototype-based learning.

## 5 Conclusion

We presented SPL, a unified framework that effectively addresses unsupervised and sparsely-supervised 3D object detection. At its core, SPL introduces a semantic-aware pseudo-labeling mechanism that robustly generates 3D supervision from images and point clouds by integrating geometric cues and temporal consistency. Beyond label generation, the framework advances representation learning through a novel multi-stage prototype training strategy, which stabilizes feature mining and enhances discriminability without direct dependency on noisy pseudo-labels. Extensive evaluations on KITTI and nuScenes demonstrate that SPL significantly outperforms existing methods in both learning paradigms, validating its capability to learn effectively from minimal or no manual annotations. For future work, we will extend the pseudo-labeling to support more diverse object categories. We also plan to develop iterative optimization strategies, such as a self-training framework that progressively refines pseudo-labels and model parameters.

## References

- Aharon, N., Orfaig, R., Bobrovsky, B.Z.: Bot-sort: Robust associations multi-pedestrian tracking. arXiv preprint arXiv:2206.14651 (2022) [6](#), [13](#)
- Azim, A., Aycard, O.: Detection, classification and tracking of moving objects in a 3d environment. In: 2012 IEEE Intelligent Vehicles Symposium. pp. 802–807. IEEE (2012) [4](#)
- Baur, S.A., Moosmann, F., Geiger, A.: Liso: Lidar-only self-supervised 3d object detection. In: European Conference on Computer Vision. pp. 253–270. Springer (2024) [2](#), [3](#), [5](#), [14](#), [15](#)
- Caesar, H., Bankiti, V., Lang, A.H., Vora, S., Liong, V.E., Xu, Q., Krishnan, A., Pan, Y., Baldan, G., Beijbom, O.: nuscenes: A multimodal dataset for autonomous driving. In: Proceedings of the IEEE/CVF conference on computer vision and pattern recognition. pp. 11621–11631 (2020) [1](#), [12](#), [13](#)
- Chen, Y., Liu, J., Zhang, X., Qi, X., Jia, J.: Voxelnext: Fully sparse voxelnet for 3d object detection and tracking. In: Proceedings of the IEEE/CVF conference on computer vision and pattern recognition. pp. 21674–21683 (2023) [15](#)

6. Deng, J., Shi, S., Li, P., Zhou, W., Zhang, Y., Li, H.: Voxel r-cnn: Towards high performance voxel-based 3d object detection. In: Proceedings of the AAAI conference on artificial intelligence. vol. 35, pp. 1201–1209 (2021) [1](#), [4](#), [8](#), [13](#)
7. Ester, M., Kriegel, H.P., Sander, J., Xu, X., et al.: A density-based algorithm for discovering clusters in large spatial databases with noise. In: kdd. vol. 96, pp. 226–231 (1996) [7](#), [13](#)
8. Geiger, A., Lenz, P., Urtasun, R.: Are we ready for autonomous driving? the kitti vision benchmark suite. In: 2012 IEEE conference on computer vision and pattern recognition. pp. 3354–3361. IEEE (2012) [1](#), [12](#), [13](#)
9. He, K., Fan, H., Wu, Y., Xie, S., Girshick, R.: Momentum contrast for unsupervised visual representation learning. In: Proceedings of the IEEE/CVF conference on computer vision and pattern recognition. pp. 9729–9738 (2020) [5](#), [11](#)
10. Ji, M., Yang, J., Zhang, S.: Enhancing pseudo-boxes via data-level lidar-camera fusion for unsupervised 3d object detection. In: Proceedings of the 33rd ACM International Conference on Multimedia. pp. 896–904 (2025) [2](#), [5](#)
11. Lang, A.H., Vora, S., Caesar, H., Zhou, L., Yang, J., Beijbom, O.: Pointpillars: Fast encoders for object detection from point clouds. In: Proceedings of the IEEE/CVF conference on computer vision and pattern recognition. pp. 12697–12705 (2019) [4](#)
12. Lee, S., Lim, H., Myung, H.: Patchwork++: Fast and robust ground segmentation solving partial under-segmentation using 3d point cloud. In: 2022 IEEE/RSJ International Conference on Intelligent Robots and Systems (IROS). pp. 13276–13283. IEEE (2022) [6](#)
13. Lentsch, T., Caesar, H., Gavrila, D.M.: Union: Unsupervised 3d object detection using object appearance-based pseudo-classes. Advances in Neural Information Processing Systems **37**, 22028–22046 (2024) [2](#), [3](#), [5](#), [15](#)
14. Li, H., Li, Y., Cao, Y., Han, Y., Jin, Y., Wei, Y.: Weakly supervised object detection with class prototypical network. IEEE Transactions on Multimedia **25**, 1868–1878 (2022) [5](#)
15. Li, Z., Guo, J., Cao, T., Bingbing, L., Yang, W.: Gpa-3d: Geometry-aware prototype alignment for unsupervised domain adaptive 3d object detection from point clouds. In: Proceedings of the IEEE/CVF international conference on computer vision. pp. 6394–6403 (2023) [5](#)
16. Liu, C., Gao, C., Liu, F., Liu, J., Meng, D., Gao, X.: Ss3d: Sparsely-supervised 3d object detection from point cloud. In: Proceedings of the IEEE/CVF conference on computer vision and pattern recognition. pp. 8428–8437 (2022) [5](#)
17. Liu, Y., Wang, T., Zhang, X., Sun, J.: Petr: Position embedding transformation for multi-view 3d object detection. In: European conference on computer vision. pp. 531–548. Springer (2022) [4](#)
18. Liu, Z., Wu, Z., Tóth, R.: Smoke: Single-stage monocular 3d object detection via keypoint estimation. In: Proceedings of the IEEE/CVF conference on computer vision and pattern recognition workshops. pp. 996–997 (2020) [4](#)
19. Liu, Z., Tang, H., Amini, A., Yang, X., Mao, H., Rus, D., Han, S.: Bevfusion: Multi-task multi-sensor fusion with unified bird’s-eye view representation. arXiv preprint arXiv:2205.13542 (2022) [1](#), [4](#), [8](#)
20. Lu, X., Diao, W., Mao, Y., Li, J., Wang, P., Sun, X., Fu, K.: Breaking immutable: Information-coupled prototype elaboration for few-shot object detection. In: Proceedings of the AAAI conference on artificial intelligence. vol. 37, pp. 1844–1852 (2023) [5](#)
21. Peng, X., Zhu, X., Ma, Y.: Cl3d: Unsupervised domain adaptation for cross-lidar 3d detection. In: Proceedings of the AAAI conference on artificial intelligence. vol. 37, pp. 2047–2055 (2023) [5](#)

22. Peterson, L.E.: K-nearest neighbor. *Scholarpedia* 4(2), 1883 (2009) 7
23. Postica, G., Romanoni, A., Matteucci, M.: Robust moving objects detection in lidar data exploiting visual cues. In: 2016 IEEE/RSJ International Conference on Intelligent Robots and Systems (IROS). pp. 1093–1098. IEEE (2016) 4
24. Reading, C., Harakeh, A., Chae, J., Waslander, S.L.: Categorical depth distribution network for monocular 3d object detection. In: Proceedings of the IEEE/CVF conference on computer vision and pattern recognition. pp. 8555–8564 (2021) 4
25. Shi, S., Guo, C., Jiang, L., Wang, Z., Shi, J., Wang, X., Li, H.: Pv-rcnn: Point-voxel feature set abstraction for 3d object detection. In: Proceedings of the IEEE/CVF conference on computer vision and pattern recognition. pp. 10529–10538 (2020) 1, 4
26. Sindagi, V.A., Zhou, Y., Tuzel, O.: Mvx-net: Multimodal voxelnet for 3d object detection. In: 2019 International Conference on Robotics and Automation (ICRA). pp. 7276–7282. IEEE (2019) 4
27. Sualeh, M., Kim, G.W.: Dynamic multi-lidar based multiple object detection and tracking. *Sensors* 19(6), 1474 (2019) 4
28. Sun, B., Liu, Y., He, H., Tian, Y., Wang, F.Y.: Annofreeod: Detecting all classes at low frame rates without human annotations. In: Proceedings of the IEEE/CVF International Conference on Computer Vision. pp. 5315–5325 (2025) 2, 3, 5, 15
29. Sun, P., Kretschmar, H., Dotiwala, X., Chouard, A., Patnaik, V., Tsui, P., Guo, J., Zhou, Y., Chai, Y., Caine, B., et al.: Scalability in perception for autonomous driving: Waymo open dataset. In: Proceedings of the IEEE/CVF conference on computer vision and pattern recognition. pp. 2446–2454 (2020) 1, 15
30. Tian, Y., Ye, Q., Doermann, D.: Yolov12: Attention-centric real-time object detectors. arXiv preprint arXiv:2502.12524 (2025) 6, 13
31. Wei, Y., Su, S., Lu, J., Zhou, J.: Fgr: Frustum-aware geometric reasoning for weakly supervised 3d vehicle detection. In: 2021 IEEE International Conference on Robotics and Automation (ICRA). pp. 4348–4354. IEEE (2021) 2, 3, 5
32. Wu, A., Han, Y., Zhu, L., Yang, Y.: Universal-prototype enhancing for few-shot object detection. In: Proceedings of the IEEE/CVF international conference on computer vision. pp. 9567–9576 (2021) 5
33. Wu, H., Lin, H., Guo, X., Li, X., Wang, M., Wang, C., Wen, C.: Motal: Unsupervised 3d object detection by modality and task-specific knowledge transfer. In: Proceedings of the IEEE/CVF International Conference on Computer Vision. pp. 6284–6293 (2025) 2, 3, 5, 14
34. Wu, H., Zhao, S., Huang, X., Wen, C., Li, X., Wang, C.: Commonsense prototype for outdoor unsupervised 3d object detection. In: Proceedings of the IEEE/CVF Conference on Computer Vision and Pattern Recognition. pp. 14968–14977 (2024) 1, 3, 5, 14
35. Xia, Q., Deng, J., Wen, C., Wu, H., Shi, S., Li, X., Wang, C.: Coin: Contrastive instance feature mining for outdoor 3d object detection with very limited annotations. In: Proceedings of the IEEE/CVF International Conference on Computer Vision. pp. 6254–6263 (2023) 2, 3, 5, 13, 14
36. Xia, Q., Ye, W., Wu, H., Zhao, S., Xing, L., Huang, X., Deng, J., Li, X., Wen, C., Wang, C.: Hinted: Hard instance enhanced detector with mixed-density feature fusion for sparsely-supervised 3d object detection. In: Proceedings of the IEEE/CVF Conference on Computer Vision and Pattern Recognition. pp. 15321–15330 (2024) 5
37. Yan, J., Liu, Y., Sun, J., Jia, F., Li, S., Wang, T., Zhang, X.: Cross modal transformer: Towards fast and robust 3d object detection. In: Proceedings of the

- IEEE/CVF international conference on computer vision. pp. 18268–18278 (2023) [1](#), [4](#)
38. Yan, Y., Mao, Y., Li, B.: Second: Sparsely embedded convolutional detection. *Sensors* **18**(10), 3337 (2018) [4](#)
  39. Yin, T., Zhou, X., Krahenbuhl, P.: Center-based 3d object detection and tracking. In: Proceedings of the IEEE/CVF conference on computer vision and pattern recognition. pp. 11784–11793 (2021) [4](#), [8](#), [13](#)
  40. You, Y., Luo, K., Phoo, C.P., Chao, W.L., Sun, W., Hariharan, B., Campbell, M., Weinberger, K.Q.: Learning to detect mobile objects from lidar scans without labels. In: Proceedings of the IEEE/CVF Conference on Computer Vision and Pattern Recognition. pp. 1130–1140 (2022) [2](#), [3](#), [5](#), [14](#)
  41. Zhang, L., Yang, A.J., Xiong, Y., Casas, S., Yang, B., Ren, M., Urtasun, R.: Towards unsupervised object detection from lidar point clouds. In: Proceedings of the IEEE/CVF Conference on Computer Vision and Pattern Recognition. pp. 9317–9328 (2023) [1](#), [3](#), [5](#), [14](#)
  42. Zhang, R., Zhang, H., Yu, H., Zheng, Z.: Approaching outside: scaling unsupervised 3d object detection from 2d scene. In: European Conference on Computer Vision. pp. 249–266. Springer (2024) [2](#), [3](#), [5](#)
  43. Zhang, X., Xu, W., Dong, C., Dolan, J.M.: Efficient l-shape fitting for vehicle detection using laser scanners. In: 2017 IEEE Intelligent Vehicles Symposium (IV). pp. 54–59. IEEE (2017) [7](#)
  44. Zhang, Y., Wang, Z., Mao, Y.: Rpn prototype alignment for domain adaptive object detector. In: Proceedings of the IEEE/CVF conference on computer vision and pattern recognition. pp. 12425–12434 (2021) [5](#)
  45. Zhao, S., Xia, Q., Guo, X., Zou, P., Zheng, M., Wu, H., Wen, C., Wang, C.: Sp3d: Boosting sparsely-supervised 3d object detection via accurate cross-modal semantic prompts. In: Proceedings of the Computer Vision and Pattern Recognition Conference. pp. 29374–29384 (2025) [5](#), [14](#)
  46. Zhao, S., Qi, X.: Prototypical votenet for few-shot 3d point cloud object detection. *Advances in neural information processing systems* **35**, 13838–13851 (2022) [5](#)
  47. Zhou, Y., Tuzel, O.: Voxelnet: End-to-end learning for point cloud based 3d object detection. In: Proceedings of the IEEE conference on computer vision and pattern recognition. pp. 4490–4499 (2018) [4](#)
  48. Zhu, Y., Hui, L., Yang, H., Qian, J., Xie, J., Yang, J.: Learning class prototypes for unified sparse-supervised 3d object detection. In: Proceedings of the Computer Vision and Pattern Recognition Conference. pp. 9911–9920 (2025) [2](#), [3](#), [5](#)